Phase transitions and rare-earth magnetism in hexagonal and orthorhombic $DyMnO_3$ single crystals

S Harikrishnan[1], S Rößler[2], C M Naveen Kumar[1], H L Bhat[1,4], U K Rößler[3], S Wirth[2], F Steglich[2], and Suja Elizabeth[1]
[1]Department of Physics, Indian Institute of Science, Bangalore-560012, India
[2] Max Planck Institute for Chemical Physics of Solids, Nöthnitzer Straße 40, 01187 Dresden, Germany
[3] IFW Dresden, Postfach 270016, D-01171 Dresden, Germany
[4] Centre for Liquid Crystal Research, Jalahalli, Bangalore-560013, India

Abstract

The floating-zone method with different growth ambiances has been used to selectively obtain hexagonal or orthorhombic $DyMnO_3$ single crystals. The crystals were characterized by X-ray powder diffraction of ground specimen and a structure refinement as well as electron diffraction. We report magnetic susceptibility, magnetisation, and specific heat studies of this multiferroic compound in both the hexagonal and the orthorhombic structure. The hexagonal $DyMnO_3$ shows magnetic ordering of Mn^{3+} (S =2) spins on a triangular Mn lattice at $T_N^{\rm Mn} = 57$ K characterized by a cusp in the specific heat. This transition is not apparent in the magnetic susceptibility due to the frustration on the Mn triangular lattice and the dominating paramagnetic susceptibility of the Dy^{3+} (S=9/2) spins. At $T_N^{\rm Dy} = 3$ K, a partial antiferromagnetic order of Dy moments has been observed. In comparison, the magnetic data for orthorhombic $DyMnO_3$ display three transitions. The data broadly agree with results from earlier neutron diffraction experiments, which allows for the following assignment: a transition from an incommensurate antiferromagnetic ordering of Mn^{3+} spins at $T_N^{\rm Mn} = 39$ K, a *lock–in* transition at $T_{\rm lock-in} = 16$ K and a second antiferromagnetic transition at $T_N^{\rm Dy} = 5$ K due to the ordering of Dy moments. Both the hexagonal and the orthorhombic crystals show magnetic anisotropy and complex magnetic properties due to $4f$-$4f$ and $4f$-$3d$ couplings.

1 Introduction

Multiferroic manganites of the type $R\mathrm{MnO_3}$ (R=rare-earth) have attracted a great deal of attention due to two main reasons: First, on the technological front multiferroics are promising materials for potential spintronic applications such as four-state memory devices [1]. For their application, however, a better understanding of their fundamental properties is necessary. Second, these materials belong to a class of complex oxides with various coupled ordering phenomena and rich phase diagrams [2, 3, 4]. Generally, $R\mathrm{MnO_3}$ crystallizes in an orthorhombic, perovskite-like structure (space group $Pnma$), if the rare-earth ionic radius is large enough, i.e. $r_R > r_{\mathrm{Dy}}$ [5]. Thus, the manganites with R = La, Pr, Nd etc. are orthorhombic, whereas the $R\mathrm{MnO_3}$ manganites for R = Y, Tm, Yb, Lu, Er with an ionic radius smaller than that of Dy usually crystallize in hexagonal structure (space group $P6_3cm$). Since the transition between hexagonal and orthorhombic crystal structure of $R\mathrm{MnO_3}$ occurs in the rare-earth series for the ionic radius of Dy or Ho, $R\mathrm{MnO_3}$ with $r_R \simeq r_{\mathrm{Dy}}$ can be synthesized in both structures by applying different growth conditions [5].

Multiferroic $R\mathrm{MnO_3}$ compounds are simultaneously ferroelectric and magnetic. Both hexagonal as well as orthorhombic $R\mathrm{MnO_3}$ exhibit multiferroic properties but the origin of the spontaneous polarisation is different in these two symmetries. In the hexagonal system, the structural distortion arising from an asymmetric coordination of oxygen around R leads to a net polarisation, as exemplified in the case of $\mathrm{YMnO_3}$ [6], and the ferroelectric transition temperatures are as high as $T_{FE} > 700$ K. Hexagonal (h-)$R\mathrm{MnO_3}$ exhibits two kinds of magnetic phase transitions: (i) an antiferromagnetic ordering of the Mn-sublattice below a Néel temperature $T_N \sim 100$ K, and (ii) a low temperature ordering of the R moments usually below 10 K [7]. The ferroelectric order persists down to low temperatures through these magnetic transitions [8], and a coupling between antiferromagnetic and ferroelectric domains has been observed by optical second harmonic generation (SHG) [9]. The crystal structure of h-$R\mathrm{MnO_3}$ essentially consists of corner-sharing $\mathrm{MnO_5}$ bipyramids separated by layers of R^{3+}. The Mn ions within the ab plane of the hexagonal structure occupy a stacked triangular lattice giving rise to an antiferromagnetic Mn-O-Mn (super-)exchange coupling between nearest Mn-neighbours [10, 11]. Below 100 K a three-dimensional ordering of the Mn spins results in an antiferromagnetic phase in h-$R\mathrm{MnO_3}$ [12]. This antiferromagnetic transition has been observed in magnetic susceptibility and specific heat of h-$R\mathrm{MnO_3}$ systems like $\mathrm{ScMnO_3}$, $\mathrm{LuMnO_3}$ and $\mathrm{YMnO_3}$ [12]. At the Néel temperature, a non-collinear 120° antiferromagnetic spin structure is established owing to the geometrical frustration of the triangular lattice planes. The coupling of these triangular lattices of Mn-layers along the c axis is difficult to resolve from macroscopic measurements but it has been investigated for various hexagonal manganites, e.g., by neutron diffraction and SHG methods [13]. The responsible and much weaker Mn-O-O-Mn super-superexchange couplings may be ferromagnetic or antiferromagnetic depending on the particular rare-earth through changes of the lattice parameters [14]. In the much-studied compound h-$\mathrm{HoMnO_3}$ from this class of materials, an antiferromagnetic coupling has been proposed from neutron diffraction [11].

Generally, the $4f$ moments of R^{3+} in h-$R\mathrm{MnO_3}$ may order at very low temperature. The interaction of the magnetic sublattices of h-$R\mathrm{MnO_3}$ poses interesting problems due to the frustration in the Mn sublattice which carries over to the coupling of R-moments within their R sublattice [9]. It should be noted that the rare-earth ions occupy two inequivalent crystallographic positions – the 2(a) and 4(b) sites denoted as $R1$ and $R2$, respectively – while the Mn ions occupy the 6(c) position. Hence, the rare-earth magnetism in h-$R\mathrm{MnO_3}$ may display multi-sublattice effects, and the ordering of the rare-earth moments in the two different crystallographic sites 4(b) and 2(a) is found to be different for different rare-earths. Moreover, the magnetic moments on these two sites can be considered to be independent and do not have to be of the same size [7, 11]. For different rare-earth ion, the geometric arrangement of the sublattice remains the same, but the low temperature magnetic properties can be different depending on the anisotropy as well as the sign and relative strength of the $4f$-$4f$ and $4f$-$3d$ couplings. However, the rare-earth moments at the 4(b) sites are usually ordered and directed perpendicular to the ab basal plane, i.e., parallel to the c-axis. Hence, the inter sublattice coupling may be frustrated too and may give rise to complex magnetic phase diagrams.

In h-$\mathrm{HoMnO_3}$ the Mn spins order at $T_N^{\mathrm{Mn}} \approx 72$ K [15] and, at temperatures below this transition, this compound displays a complex magnetic phase diagram (as studied recently by Lorenz *et al.* [16]). The lattice anomalies introduced by the magnetoelastic interactions of the novel magnetic phases in $\mathrm{HoMnO_3}$ are also reflected in dielectric measurements as anomalies [17]. The fact that the magnetic structure of this class of $R\mathrm{MnO_3}$ is complex and poorly understood is reinstated by the ongoing attempts to determine the magnetic structure and the magnetic phase diagram including an intricate succession of field-induced

phases in $HoMnO_3$ [18, 19]. In comparison, relatively little is known about the magnetism of h-$DyMnO_3$ [20]. Therefore, a detailed investigation on hexagonal $DyMnO_3$ may provide further insight into the magnetism of this class of materials.

In orthorhombic (o-)$R$$MnO_3$ multiferroics with perovskite-like crystal structure the ferroelectricity is attributed to a complex spiral spin-order that breaks the inversion symmetry [21, 22]. The associated magnetically driven transitions usually occur at much lower temperatures. o-$DyMnO_3$ has been investigated in some detail mainly by diffraction methods, and hence, detailed microscopic information on the spin-structure is available [23, 24, 25, 26]. An incommensurate ordering of Mn moments sets in at $T_N^{\rm Mn} = 39$ K. The collinear magnetic order is of a longitudinal sinusoidal spin-density-wave type with moments along the b-axis in the $Pbnm$ space group setting and a propagation vector $(0, q_{\rm Mn}, 0)$ that varies with temperature below $T_N^{\rm Mn}$ [23, 24]. At $T_{\rm lock-in} = 18$ K, an additional component of the Mn moment along the c axis gives rise to a spiral (cycloidal) magnetic order and breaks the inversion symmetry [25, 26]. At this temperature, spontaneous electric polarization is observed along the c axis. This electric polarization undergoes a flop transition from the c to the a axis when a magnetic field is applied within the ab plane. Below $T_N^{\rm Dy} = 5$ K, the Dy moments order in a commensurate structure with propagation vector along b [23]. Strong structural distortions related to the ordering of Mn and Dy magnetic moments and couplings between these moments have been observed by synchrotron x-ray diffraction (XRD) and resonant magnetic scattering experiments [23].

Here, we report magnetic susceptibility, magnetisation and specific heat measurements on both h-$DyMnO_3$ and o-$DyMnO_3$ single crystals. Different crystal growth atmospheres have been used to stabilize the system in one of these two crystal structures. The macroscopic measurements of magnetic properties and specific heat broadly agree with the microscopic information on the spin structure and magnetic phase transitions in the $DyMnO_3$ system. The results in particular show that the Dy magnetic moments at low temperatures are only partially ordered in the case of h-$DyMnO_3$, whereas they are completely ordered in the case of the o-$DyMnO_3$.

2 Experimental

Single crystals of $DyMnO_3$ were grown by the optical floating-zone method in an infrared furnace (FZ-T-10000-H-VI-VP procured from Crystal Systems Inc.). The furnace is equipped with four hemi-ellipsoidal mirrors and halogen lamps that are capable of delivering a total power of 6 kW. The starting materials for growth were prepared following the standard route of solid state reaction. The precursors Dy_2O_3 and MnO_2 were mixed intimately and subsequently heat treated at 1200^0C for 12 h. Then, the material was reground and annealed again at 1250^0C for 24 h. This process was repeated until a single phase was obtained. X-ray diffraction (XRD) was performed to confirm phase purity. The powder was used to fabricate ceramic ingots for crystal growth by filling it into rubber tubes and subjecting them to a hydrostatic pressure of 70 MPa. These cylindrical ingots were sintered at 1450^0C for 12 h prior to growth. During the growth the seed and feed rods were rotated at 40 rpm in opposite directions. At a growth rate of 4 - 6 mm/h crystals of typical dimensions 5 cm length and 4 mm - 6 mm diameter were obtained. Growth was performed in the ambiance of either argon or air, to obtain either hexagonal or orthorhombic crystals, respectively. It should be noted that the Gibb's free energy of the two polymorphic modifications of $DyMnO_3$ are close [20] and though the perovskite phase is stable at room temperature, a transformation to a hexagonal phase is possible at temperatures greater than 1600°C [27]. It is documented that the synthesis in oxygen leads to the formation of a perovskite phase whereas oxygen deficit leads to the hexagonal phase [28]. In an oxygen-deficient atmosphere the crystal will be unable to complete the twelve-fold coordination of R required for the perovskite; instead an eight-fold coordination with hexagonal symmetry results. Laue photographs of the grown crystals indicated their single crystalline nature. Chemical composition of these crystals was determined by energy dispersive X-ray analysis (EDAX) as well as by inductively coupled atomic emission spectroscopy (ICPAES) using a Perkin Elmer Spectrometer Optima 2000. Powder X-ray diffractograms of pulverized samples were obtained from a Philips X'Pert diffractometer with Cu-Kα radiation ($\lambda = 1.54$ Å). Slow scans with a resolution of 0.01° were obtained in the range $2\theta = 5$–$100°$. Crystal structure refinement was performed by the Rietveld method [29] using the FULLPROF code [30]. Selected area electron diffraction (SAED) patterns were obtained through transmission electron microscopy using a Tecnai G 30 electron microscope. Magnetic measurements were conducted on oriented single crystals in a commercial (Quantum Design) superconducting quantum

interference device magnetometer (SQUID) in the temperature range 2 K – 300 K. Magnetic susceptibility and specific heat measurements were performed using a physical property measurement system (Quantum Design).

3 Results and discussion: Hexagonal $DyMnO_3$

3.1 Crystal structure

As-grown crystals of both *h,o*-$DyMnO_3$ were black and lustreless. The XRD data for *h*-$DyMnO_3$ and results of the Rietveld analysis are displayed in figure 1. The crystal structure has been refined in a hexagonal space group $P6_3cm$. The refined lattice parameters are $a = 6.189(1)$ Å and $c = 11.461(4)$ Å. Previous structural studies on *h*-$R$$MnO_3$ report the structure in $P6_3cm$ space group with similar values for the lattice parameters [5]. The indexed SAED pattern, figure 2, confirms the structure refinement by the Rietveld method.

3.2 *DC* Magnetisation

The field cooled (FC) as well as zero field cooled (ZFC) magnetisation curves at a field of 10 Oe applied along the c axis presented in figure 3(a) show bifurcation at about 3 K. Similar data obtained for field applied perpendicular to the c axis are shown in the inset of figure 3(a). The temperature evolution of magnetisation is different from the properties reported for *h*-$HoMnO_3$ or *h*-$ScMnO_3$ where such a bifurcation at low temperature was not visible [11, 31]. It is interesting to note that the antiferromagnetic transition of Mn at $T_N^{\mathrm{Mn}} = 57$ K, (determined from specific heat measurements) is not discernible in the magnetisation profile of *h*-$DyMnO_3$. At temperatures above T_N^{Mn}, the inverse susceptibility $1/\chi$ follows a Curie-Weiss behaviour, yielding an effective magnetic moment value $\mu_{\mathrm{obs}} = 10.81\ \mu_B$(figure 4(b)). This moment is close to the expected value $\mu_{\mathrm{nom}} = [\mu^2_{\mathrm{eff}}(\mathrm{Mn})+\mu^2_{\mathrm{eff}}(\mathrm{Dy})]^{1/2} = 11.67\ \mu_B$. The Weiss temperature obtained from the fit is $\theta_W \approx -23$ K. The negative value of θ_W indicates the presence of antiferromagnetic exchange interactions. The values of μ_{obs} and θ_W agree well with those ($10.7\mu_B$ and -17 K) obtained for similar *h*-$HoMnO_3$ crystals [11]. However, as the magnetic response in the paramagnetic regime is strongly influenced by excitations of the $4f$-electrons of Dy split by the crystalline electric field (CEF), the parameters from the Curie-Weiss fit do not directly relate to the physics of the coupled magnetic sublattices as in other hexagonal $R$$MnO_3$ systems [7].

The isothermal magnetisation curves at 2, 10 and 60 K measured along the c axis and within the ab plane are presented in figure 4(a). For $T \geq 10$ K the magnetisation and initial susceptibility for fields applied in the ab plane is larger than those measured along the c axis. This is consistent with (i) the easy-plane character of the non-collinear magnetic order in the triangular Mn-sublattice, (ii) the easy-axis anisotropy introduced by the Dy-ions along the c-axis. The data for 10 K and 60 K do not show any remanent magnetisation, thus spontaneous or weak ferromagnetic moments are absent at these temperatures. The overall magnetisation increase for this temperature range is probably dominated by a large linear contribution from the paramagnetic Dy moments. At 2 K, a ferromagnetic-like hysteretic behaviour is found in the low-field part of the magnetisation curve (figure 4 (b)) and the initial susceptibility is stronger along the c axis than along the ab plane. The magnetic behavior at this low temperature must be attributed to the Dy-magnetic order and is strongly anisotropic. The magnetisation curve along c has the character of a ferromagnetic easy-axis system with technical saturation reached at about 600 Oe. In order to estimate the zero-field magnetic moment we extrapolated the linear part of $M(H)$ above 600 Oe towards zero field and obtained $M_S = 7.5$ emu/g $= 0.36\ \mu_B$/f.u.. Assuming that this spontaneous magnetisation is only due to a ferromagnetic contribution of the Dy-moments on the 2(a) sites, still the observed value for the ordered magnetic moment is very small, only about 0.1 times the full polarization on the 2(a)-sites. Hence, it is likely that the Dy-moments responsible for this effect are only partially polarized by a coupling to the Mn-sublattice and/or the 4(b)-sublattice, e.g. by dipolar couplings. Superimposed on this essentially ferromagnetic behaviour with a small saturation magnetisation is a linear overall increase at low fields 600 Oe $< H <$ 20 kOe and a tendency towards lower high–field susceptibility, although no saturation is attained even at 50 kOe. Correspondingly, the magnetisation curve along the ab plane resembles a hard-axis magnetisation process with an essentially linear increase of magnetisation. However, the small hysteresis seen in the ab magnetisation curve cannot be explained by this process. The existence of the different, yet coupled sublattices of Mn and Dy, as mentioned above, underlies the high magnetic anisotropy and the complex magnetisation behavior in this crystal.

A preliminary qualitative picture of the magnetic structure of h-$DyMnO_3$ based on the magnetic measurements is possible by a 'three sub-lattice model' [7]. This model assumes three different and largely decoupled magnetic sublattices in h-$RMnO_3$: a lattice of Mn (at 6c) that forms a 120^0 spin arrangement in the ab plane, and two more lattices formed by the rare-earth ions $R1$ and $R2$ situated at 2(a) and 4(b) sites, respectively. A schematic of the arrangement is shown in figure 5.

As the temperature is reduced, at around 57 K, the interlayer coupling between the Mn ions in the ab plane gives rise to a non-collinear AF order, as found by specific heat data (see below). However, the exchange field originating from the Mn order below T_N^{Mn} acts on the rare-earth lattice, and with further reduction in temperature, the $R1$ and $R2$ moments commence to order. In the case of $DyMnO_3$, the Dy^{3+} moments order below $T_N^{\mathrm{Dy}} = 3$ K. At 2 K, a ferromagnetic feature is detected when measuring along c axis whereas along the ab plane the ferromagnetic component is weak. In analogy to $ErMnO_3$ [7] this suggest that the rare-earth ions at $R1$ could be paramagnetic down to low temperatures before they order ferromagnetically. On the other hand, the $R2$ ions may order antiferromagnetically with their magnetic moments pointing along the hexagonal c axis similar to the magnetic order observed in $YbMnO_3$ and $TmMnO_3$ [12]. With further increase in magnetic field, at about 30 kOe, the bending in the $M(H)$ curves for both directions of applied fields signals a gradual saturation at 2 and 10 K. There is no clear explanation for this effect, however, it should be noted that a contribution of the Mn-sublattice is likely, as a similar bending of $M(H)$ curves has been observed for h-$YMnO_3$ with a non-magnetic R-site at low temperatures [31].

3.3 AC-Susceptibility

Recently, observations on thin films of h-$DyMnO_3$ indicated that the competition and frustration inherent in the magnetic multi-sublattice of $RMnO_3$ may lead to a magnetic spin-glass state [32]. However, from the ac-susceptibility of h-$DyMnO_3$ along c and ab the transition of the Mn lattice is not obvious and possibly being masked by the frustration in the Mn lattice or by the strong Dy paramagnetic susceptibility. It is clear that the competing inter- and intra-sublattice couplings are present in the hexagonal structure of $RMnO_3$ which can have pronounced effects at low temperatures. As expected, the real part of the susceptibility, χ', exhibits a peak close to 3 K which is evident in the $\chi'(T)$ curves of h-$DyMnO_3$ for the range of frequencies 133 Hz – 10 kHz measured along the c axis as well as the ab plane, figure 6(a) and (b), respectively. This peak originates from the ordering of Dy moments at low temperature. The peak temperature displays no significant dependence on frequency. This rules out the presence of slow dynamics as a characteristics of glassy magnetism.

Figure 7(a) demonstrates the effect of magnetic field on χ' for fields up to 70 kOe. With the application of a magnetic field along c-axis, the antiferromagnetic signal is suppressed and the peak at 3 K diminishes in magnitude. Above 30 kOe, the peak vanishes corroborating a gradual field-driven transformation of the magnetic structure in this field range. When a magnetic field is applied along the ab plane (figure 7(b)), one observes a shift in the peak to higher temperatures, in addition to a decrease in the magnitude of χ'.

3.4 Specific heat

The specific heat C_p of h-$DyMnO_3$ measured at zero applied field is presented in figure 8 (inset magnifies the two apparent transitions). The antiferromagnetic transition of the Mn sublattice is evident as a sharp peak at about 57 K. Thus, in h-$DyMnO_3$ the magnetic ordering transition in the Mn-sublattice appears only in specific heat, but is not detectable in the magnetic susceptibility data. This is in contrast to the properties of hexagonal $HoMnO_3$, where T_N^{Mn} is detected by peaks in C_p and in χ'' as well [11]. In contrast to the specific heat of h-$HoMnO_3$ studied by Muñoz *et al.* [33], no sign of a Mn reorientation in the basal plane at intermediate temperatures is observed in h-$DyMnO_3$. At 3 K, a second peak is observed in the specific heat corresponding to the ordering of Dy-moments.

4 Results and discussion: Orthorhombic $DyMnO_3$

4.1 Crystal structure

Generally, the *o*-$R$$MnO_3$ derives from the perovskite structure [24]. The powder XRD data for *o*-$DyMnO_3$ used for the structural analysis are displayed in figure 9 along with the Rietveld refinement in the *Pnma* space group. The lattice parameters obtained are a = 5.832(1) Å, b = 7.381(2) Å and c = 5.280(1) Å, respectively. Earlier structural studies [34] on single crystalline $DyMnO_3$ reported similar values. The structure solution obtained for *o*-$DyMnO_3$ is also supported by the SAED pattern, figure 10, which could be indexed in the orthorhombic structure. The perovskite $DyMnO_3$ presents a highly distorted structure owing to the small value of the ionic radius r_R of Dy at the R site, the tolerance factor of $DyMnO_3$ being about 0.85. The lattice distortions – Jahn Teller distortion and octahedral rotation – observed in perovskite $R$$MnO_3$ evolve continuously with decreasing r_R [35]. Nevertheless, such a smooth evolution of distortions with r_R does not imply a similarly continuous evolution of the magnetic structure [36]. Normally, a reduction in r_R is followed by a deviation of the Mn–O–Mn bond angle from 180°, thereby distorting the major magnetic exchange path. In turn, the magnetic structure of $R$$MnO_3$ changes from A type to E type as a function of r_R [35, 36]. However, smaller rare-earths like Dy, Tb and Gd fall in the intermediate region of bond angle values that stabilize incommensurate magnetic structures [37].

4.2 *DC* Magnetisation

The Mn magnetic moments in the perovskite $DyMnO_3$ are directed along the orthorhombic *b*-axis [25]. Below $T_N \approx 40$ K the Mn spins enter the incommensurate state where they order sinusoidally with modulation vector along (0, q_{Mn}, 0) [38, 39]. Based on neutron scattering measurements [22] it is further reported that the sinusoidal order transforms into an incommensurate spiral order through a *lock–in* transition at $T_{lock-in} = 18$ K. At even lower temperature the rare-earth spins also order, $T_N^{Dy} \approx 6$ K.

The magnetisation curves obtained in FC and ZFC cycles with an applied field of 20 Oe parallel to *b* axis are presented in figure 11(a). Three features can be recognized from these curves; a bifurcation in FC/ZFC cycles at $T_{split} \approx 45$ K (magnified in the second inset for clarity), a peak in the ZFC curve at 16 K, and an inflection in the FC magnetisation curve at 5 K. These features can be attributed to the incommensurate Mn-spin order, to the *lock–in* transition, and to the Dy-spin order, respectively. Values of T_N^{Dy} at 9 and 6 K have been reported for polycrystalline [37] and single crystal samples of $DyMnO_3$, respectively [25]. At higher fields, the ZFC magnetisation curve exhibits a peak at lower temperature around 7 K, figure 11(b). However, no signature of the ordering transition into the incommensurate structure at 39 K is visible. Interestingly, the low temperature rise in ZFC magnetisation persists even in an applied field of 1000 Oe. The $1/\chi$ data (not shown) above T_N follow a Curie-Weiss behaviour yielding a value of 13.67 μ_B for μ_{obs}. This is higher than the expected value $\mu_{nom} = 11.67$ μ_B calculated from $\mu_{nom} = [\mu_{eff}^2(Mn) + \mu_{eff}^2(Dy)]^{1/2}$. From the fit, $\theta_W \approx -20$ K which again indicates the presence of antiferromagnetic interactions in the system. However, as in the case of *h*-$DyMnO_3$, the parameters of the Curie-Weiss law do not reflect the properties of a simple paramagnetic and coupled system since they are affected by the transitions between the CEF-levels of Dy.

The low temperature behaviour of the magnetisation measured perpendicular to the *b* axis is substantially different from that parallel to *b*, as can be inferred from figure 12(a) and (b). Here, the FC/ZFC curves at 10 and 1000 Oe, respectively, are presented. Even though the bifurcation signalling the first transition into the incommensurate structure and the *lock–in* transition are evident (see also the insets of figure 12 (a)), both the FC and ZFC curves show a decrease of the magnetisation below the peak at ≈ 7 K. This is different from the low temperature behaviour of the magnetisation parallel to *b* and indicates that the magnetic easy axis of the orthorhombic system is along the *b* axis. Although the absolute magnitude of magnetisation is higher in this case, the difference between FC and ZFC is less pronounced.

Isothermal magnetisation curves at 2, 10 and 60 K with applied field parallel to the *b* axis are presented in figure 13. No hysteresis is discernible and the magnetisation varies linearly with applied field. In the related compound $HoMnO_3$, Muñoz *et al.* found a metamagnetic transition at 2 K for fields higher than 50 kOe [33]. In *o*-$DyMnO_3$, no such feature is observed at 2 K. It is interesting to note that the ordering temperature of the same rare-earth ion in *h*-$DyMnO_3$ (3 K) and *o*-$DyMnO_3$ (7 K) are separated by about 4 K.

4.3 *AC*-Susceptibility

The dependence of χ' on temperature at different probing frequencies for o-$DyMnO_3$ is presented in figure 14(a). The measurement was performed with applied field parallel to the b axis. Although a weak dependence of χ' on frequency is observed, the shift in the peak temperature T_{peak} is very small ($\sim$ 1 K). This peak corresponds to the $T_{\mathrm{lock-in}}$. Both the incommensurate transition of the Mn-spins and the antiferromagnetic transition of Dy spins are not visible in the *ac*-susceptibility. Application of a magnetic field suppresses this magnetic peak and, at the same time, shifts T_{peak} to lower temperature, figure 14(b). The change of the low-temperature peak in χ' possibly indicates a metamagnetic transition in the Dy spins. A non-collinear arrangement can give rise to additional ferroelectric displacements through magnetoelastic couplings [40].

4.4 Specific heat

The heat capacity C_p of o-$DyMnO_3$ measured in zero field is shown in figure 15. A sharp peak at about 39 K marks the antiferromagnetic transition into the sinusoidal incommensurate phase. Additional anomalies in C_p are observed at 16 K and 5 K which, again, indicate the *lock–in* transition and T_N^{Dy}. Therefore, the specific heat data corroborate the main features of the phase diagram and magnetic ordering in o-$DyMnO_3$.

5 Conclusions

We have successfully synthesized the multiferroic crystal $DyMnO_3$ in the much studied orthorhombic symmetry as well as in the less studied hexagonal symmetry by employing different growth ambiences. The basic magnetic properties were investigated by means of *dc* magnetisation, *ac*-susceptibility, and specific heat.

$h-DyMnO_3$:

Hexagonal $DyMnO_3$ shows an antiferromagnetic transition at 57 K clearly discernible in the specific heat measurement. The huge paramagnetic susceptibility stemming from Dy and/or the frustrated Mn lattice could be the reason for this transition not being visible in the magnetization and susceptibility curves. The rare-earth moment manifests itself through a partial antiferromagnetic order in the FC/ZFC curves at 3 K. The mixed interactions and frustration in the magnetic lattice do not lead to a magnetic glassy state, as is inferred from the absence of any frequency dependence in χ'. On application of a magnetic field the antiferromagnetic signal in χ' at low temperature is suppressed. In addition to the transition in the Mn sublattice the specific heat data exhibit a peak at even lower temperature resulting from the rare-earth magnetic ordering. No sign of a Mn-reorientation transition is detected in the specific heat measurement.

$o-DyMnO_3$:

DC magnetisation measurements parallel and perpendicular to the b axis markedly differ in the case of o-$DyMnO_3$ from its hexagonal counterpart. Parallel to b, the transition into the incommensurate phase is observed in the FC and ZFC curves. These curves split at 39 K, exhibit a peak in the ZFC magnetisation curve at 16 K, and a weak feature at 5 K the latter signalling the Dy order. Perpendicular to b, peaks are observed both in the FC/ZFC magnetisation curves at 7 K. *AC* susceptibility measurements do not show any signatures of the incommensurate transition or any frequency dependence. However, they clearly reflect the *lock–in* transition. The specific heat curves corroborate these conclusions displaying peaks at temperatures corresponding to the sinusoidal ordering of Mn moments into an incommensurate phase, the *lock–in* transition, and the ordering of the rare-earth moments.

Our detailed magnetisation measurements highlight the complex interplay of the 3d and rare-earth magnetism in h- and o-$DyMnO_3$. In turn, investigating the effect of rare-earth magnetism of Dy on the magnetic ordering and dielectric property of o-$DyMnO_3$ at low temperature is called for.

Acknowledgment

We thank G. Behr (IFW Dresden) for help with single-crystal orientation. The authors acknowledge the Department of Science and Technology (DST), India for OFZ crystal growth facility set up through FIST programme. SE and HLB thank DST for financial support through a project grant.

References

[1] Bibes M, Barthélémy A 2008, *Nature Materials* **7** 425

[2] Gajek M, Bibes M, Fusil S, Bouzehouane K, Fontcuberta J, Barthélémy A, Fert A 2007 *Nature Materials* **6** 296

[3] Eerenstein W, Mathur N D, Scott J F, 2006 *Nature* **442** 759

[4] Prellier W, Sing M P, Murugavel P 2005 *J. Phys.:Condens. Matter* **17** R803

[5] Zhou J -S, Goodenough J B, Gallardo-Amores J M, Morán E, Alario-Franco M A, Caudillo R 2006 *Phys. Rev. B* **74** 014422

[6] Lee S, Pirogov A, Han J H, Park J -G, Hoshikawa A, Kamiyama T 2005 *Phys. Rev. B* **71** 180413

[7] Tomuta D G *Investigations of hexagonal manganites with magnetic and non magnetic rare earths* 2003 PhD thesis, Leiden University.

[8] Lonkai Th, Tomuta D G, Amann U, Ihringer J, Hendrikx R W A, Tóbbens D M, Mydosh J A 2004 *Phys. Rev. B* **69** 134108

[9] Fiebig M, Degenhardt C and Pisarev R V 2002 *Phys. Rev. Lett.* **88** 027203

[10] Bertaut E F, Mercier M 1963 *Phys. Lett.* **5** 27

[11] Muñoz A, Alonso J A, Martìnez-Lope M J, Casáis M T, Martìnez J L, Fernàndez-Dìaz M T 2001 *Chem. Mater.* **13** 1497

[12] Tomuta D G, Ramakrishnan S, Nieuwenhuys G J, Mydosh J A 2001 *J. Phys.: Condens. Matter* **13** 4543

[13] Fiebig M, Fröhlich D, Kohn K, Leute St, Lottermoser Th, Pavlov V V, Pisarev R V 2000 *Phys. Rev. Lett.* **84** 5620

[14] Lonkai Th, Tomuta D G, Hoffmann J -U, Schneider R, Hohlwein D, Ihringer J 2003 *J. Appl. Phys.* **93** 8191

[15] Vajek O P, Kenzelmann M, Lynn J W, Kim S B, Cheong S -W 2005 *Phys. Rev. Lett.* **94** 087601

[16] Lorenz B, Yen F, Gospodinov M M, Chu C W 2005 *Phys. Rev. B* **71** 014438

[17] Yen F, dela Cruz C R, Lorenz B, Sun Y Y, Wang Y Q, Gospodinov M M, Chu C W 2005 *Phys. Rev. B* **71** 180407

[18] Brown P J, Chatterji T 2008 *Phys. Rev. B* **77** 104407

[19] Nandi S, Kreyssig A, Tan L, Kin J W, Yan J Q, Lang J C, Haskel D, McQueeney R J, Goldman A I 2008 *Phys. Rev. Lett.* **100** 217201

[20] Ivanov V Yu, Mukhin A A, Prokhorov A S, Balbashov A M, Iskhakova L D 2006 *Physics of the Solid State* **48** 1726

[21] Cheong S -W, Mostovoy M 2007 *Nature Materials* **6** 13

[22] Kimura T, Goto T, Shintani H, Ishizaka K, Arima T, Tokura Y 2003 *Nature* **426** 55

[23] Feyerherm R, Dudzik E, Aliouane N, and Argyriou D N 2006 *Phys. Rev. B* **73** 180401(R)

[24] Kimura T, Lawes G. Goto T, Tokura Y and Ramirez A P 2005 *Phys. Rev. B* **71** 224425

[25] Prokhnenko O, Feyerherm R, Dudzik E, Landsgesell S, Aliouane N, Chapon L C, and Argyriou D N 2007 *Phys. Rev. Lett.* **98** 057206

[26] Goto T, Kimura T, Lawes G, Ramirex A P, and Tokura Y 2004 *Phys. Rev. Lett.* **92** 257201

[27] Szabo G, Paris R A 1969 *C. R. Seances Acad. Sci., Ser. C* **268** 513

[28] Alonso J A, Martinez-Lope M J, Casais M T, Fernandez-Diaz M T 2000 *Inorg. Chem.* **39** 917

[29] Rietveld H M 1969 *J. Appl. Cryst.* **2** 65

[30] Rodriguez-Carvajal J 1993 *Physica B* **192** 55-69

[31] Muñoz A, Alonso J A, Martínez-Lope M J, Casáis M T, Martínez M T, Fernández-Díaz M T 2000 *Phys. Rev. B* **62** 9498

[32] Lee J H, Murugavel P, Lee D, Noh T W, Jo Y, Jung M -H, Jang K H, Park J -G 2007 *Appl. Phys. Lett* **90** 012903

[33] Muñoz A, Casáis M T, Alonso J A, Martìnez-Lope M J, Martìnez J L, Fernàndez-Dìaz M T 2001 *Inorg. Chem.* **40** 1020

[34] Mori T, Aoki K, Kamegashira N, Shishido T, Fukuda T 2000 *Materials Letters* **42** 387

[35] Tachibana M, Shimoyama T, Kawaji H, Atake T, Takayama-Muromachi E 2007 *Phys. Rev. B* **75** 144425

[36] Zhou J -S, Goodenough J B 2006 *Phys. Rev. Lett.* **96** 247202

[37] Kimura T, Ishihara S, Shintani H, Arima T, Takahashi K T, Ishizaka K, Tokura Y 2003 *Phys. Rev. B* **68** 060403(R)

[38] Ye F, Lorenz B, Huang Q, Wang Y Q, Sun Y Y, Chu C W, Fernandez-Baca J A, Dai P, Mook H A 2007 *Phys. Rev. B* **76** 060402(R)

[39] Kajimoto R, Yoshizawa H, Shintani H, Kimura T, Tokura Y 2004 *Phys. Rev. B* **70** 012401

[40] Mostovoy M 2006 *Phys. Rev. Lett.,* **96** 067601

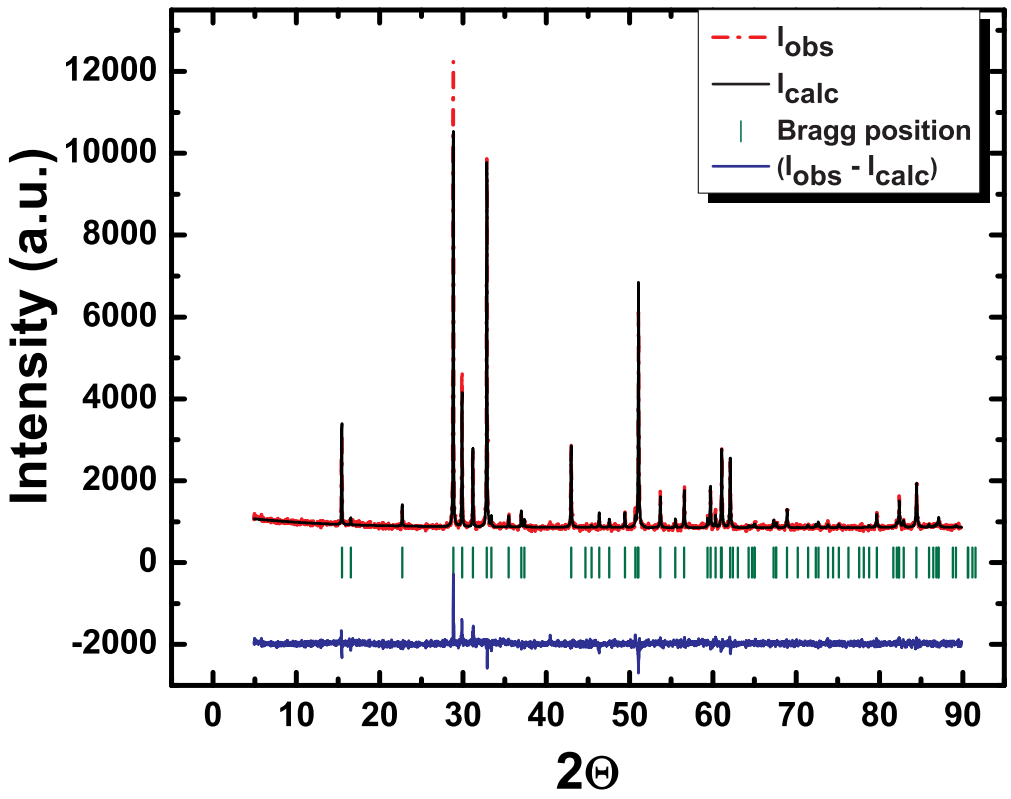

Figure 1: Powder X-ray diffraction pattern (I_{obs}) and Rietveld refinement (I_{calc}) of h-$DyMnO_3$.

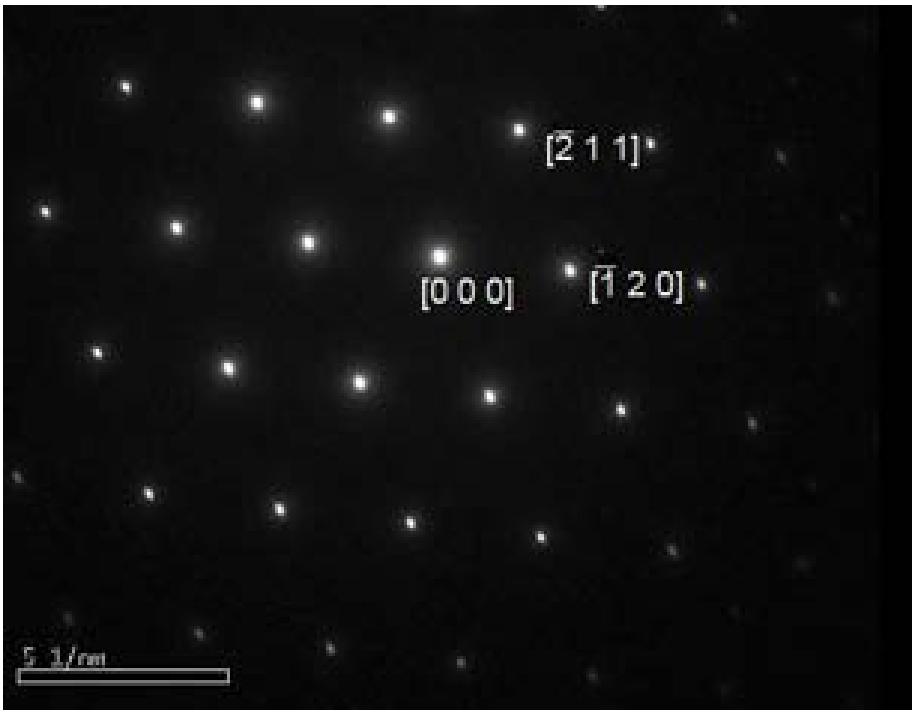

Figure 2: SAED pattern of h-$DyMnO_3$. The scale bar shows 5 nm^{-1}.

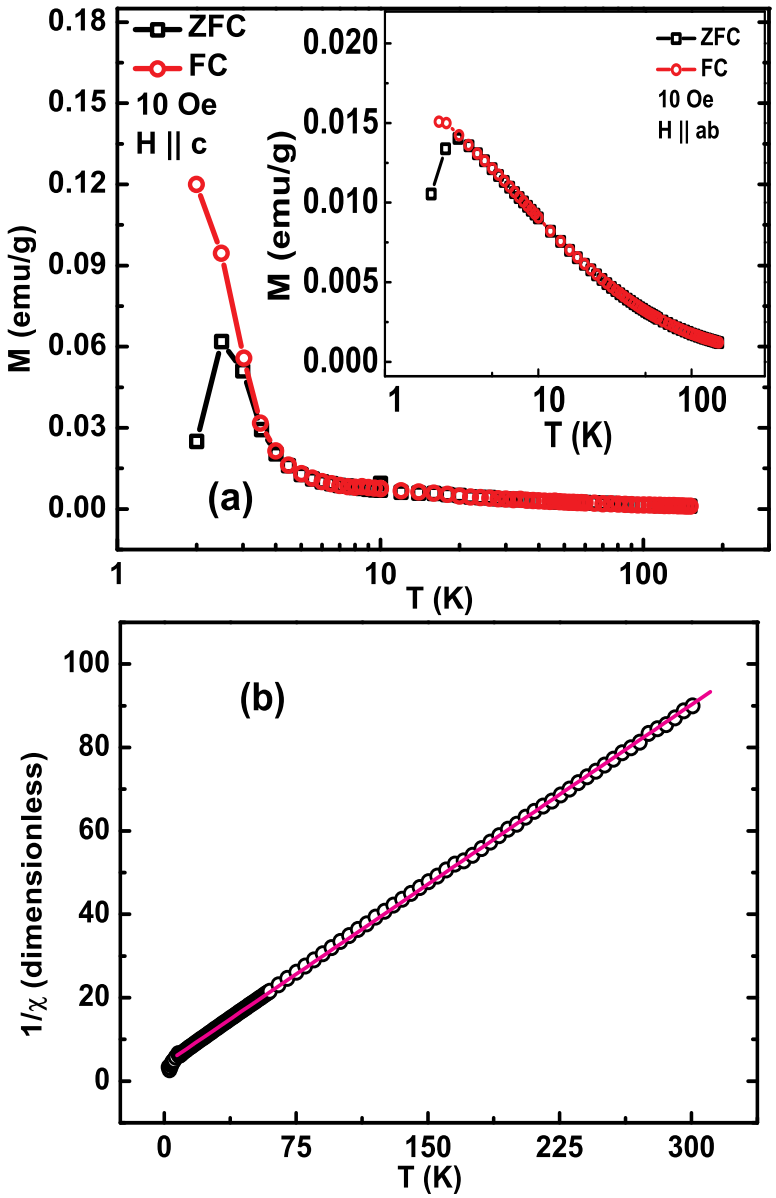

Figure 3: (a) Magnetisation of h-$DyMnO_3$ along the c axis and the ab plane (inset). The value of magnetisation is an order of magnitude higher along the c-axis. (b) A Curie-Weiss law fits the inverse susceptibility data with a negative Weiss temperature and deviations at lowest temperatures.

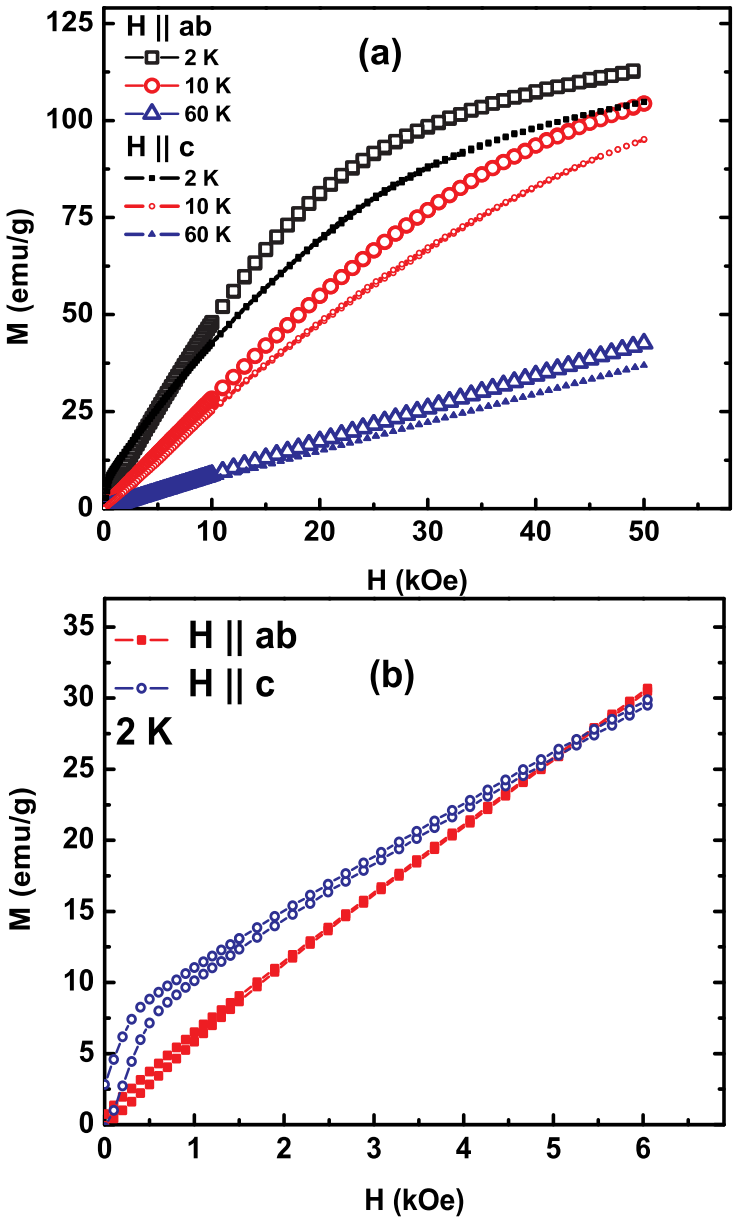

Figure 4: (a) Magnetisation isotherms of h-$DyMnO_3$ at 2, 10 and 60 K measured along c and ab directions. (b) Low-field magnetisation along c showing a weak spontaneous magnetic moment and hysteretic behaviour.

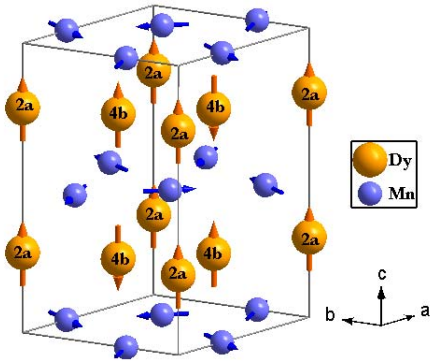

(a)

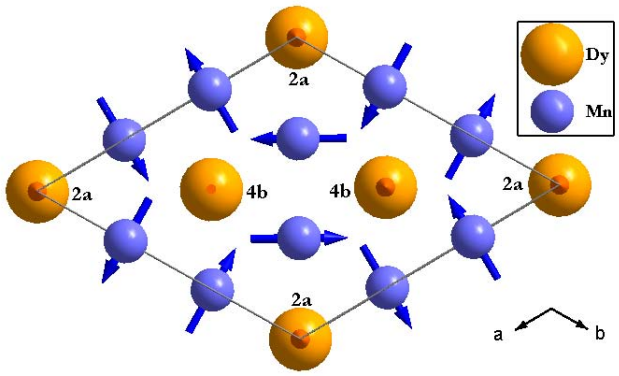

(b)

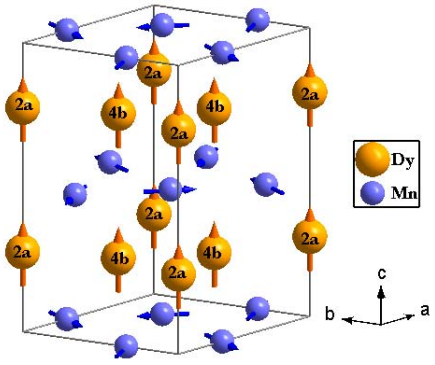

(c)

Figure 5: Magnetic structure of the hexagonal $DyMnO_3$ crystal. The Dy^{3+} ions at the two inequivalent positions along with the Mn ions are shown. Note that, although the moments at 2(a) sites are depicted as ferromagnetically aligned, the spins at this site are only partially polarized. (a) and (b) display the zero-field case while (c) presents the magnetic lattice above 30 kOe.

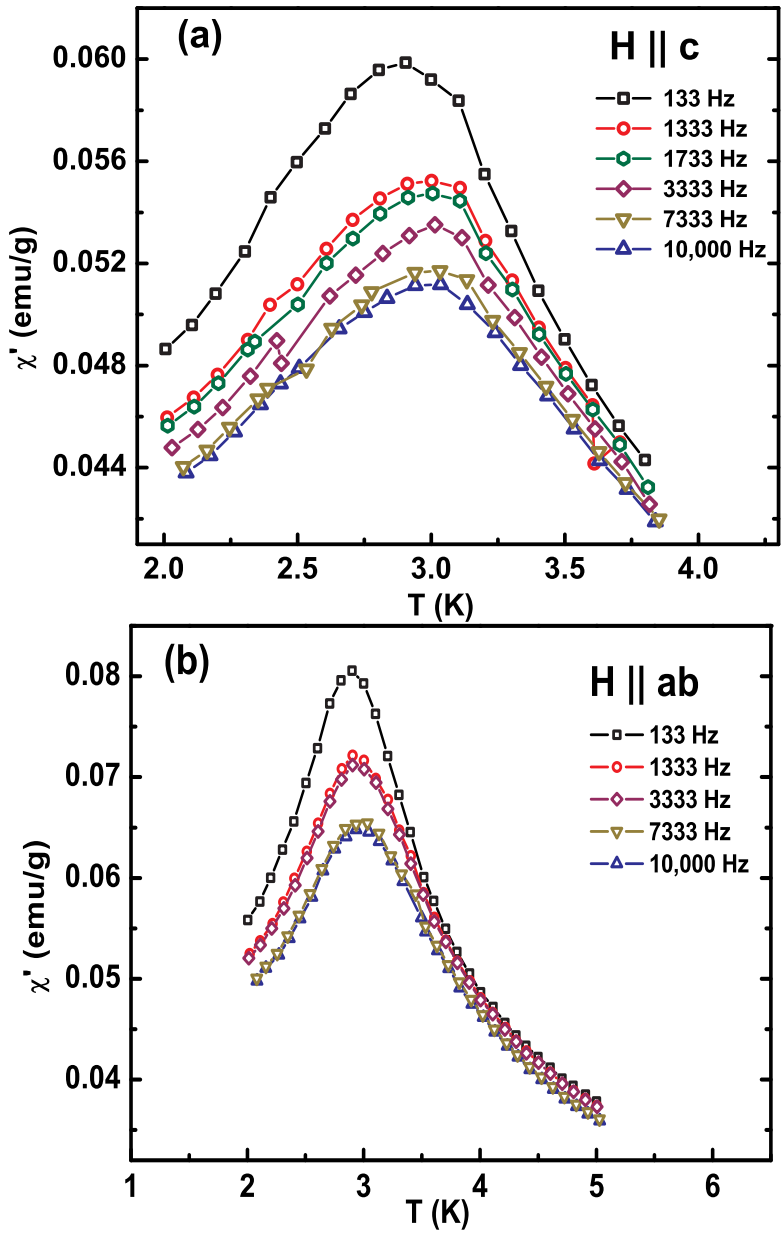

Figure 6: *AC* susceptibility curves for h-$DyMnO_3$ with magnetic field H along (a) the c axis and (b) the ab plane at different frequencies. The amplitude of the ac field was 10 Oe. There is only a very feeble dependence of the peak temperature on frequency.

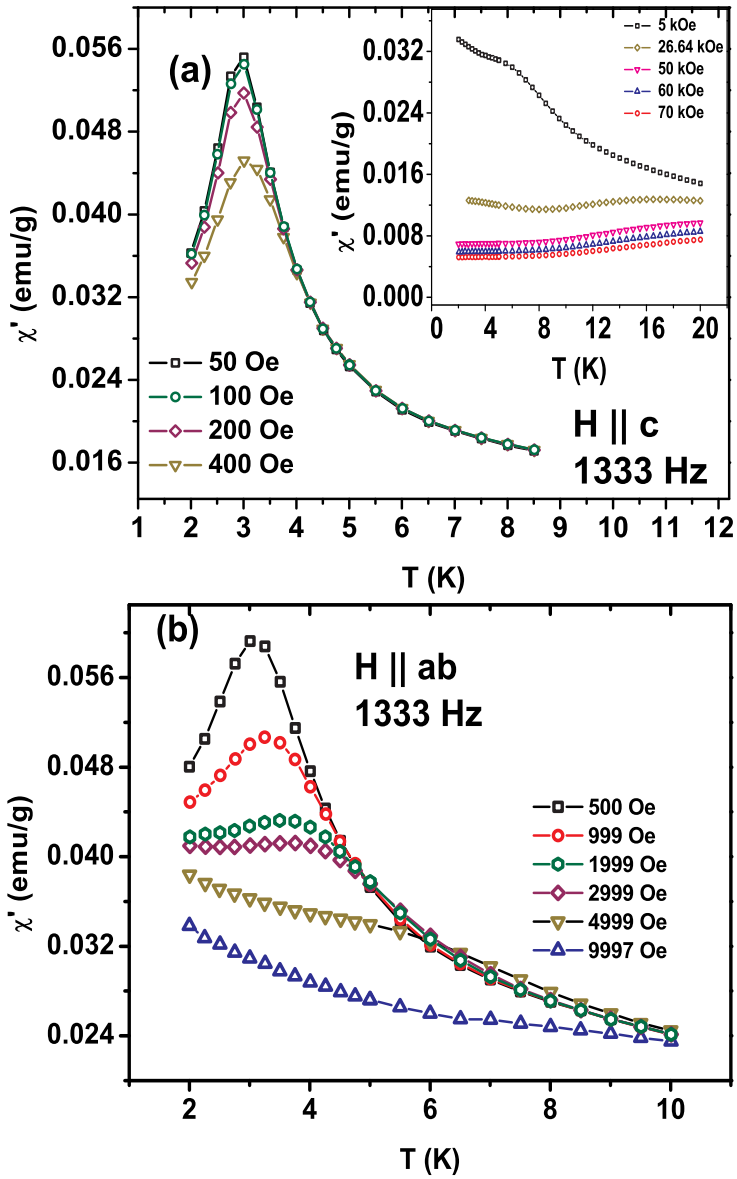

Figure 7: Effect of an imposed magnetic field H on the susceptibility of h-$DyMnO_3$ with H along (a) the c axis and (b) the ab plane. The amplitude of the ac field was 10 Oe.

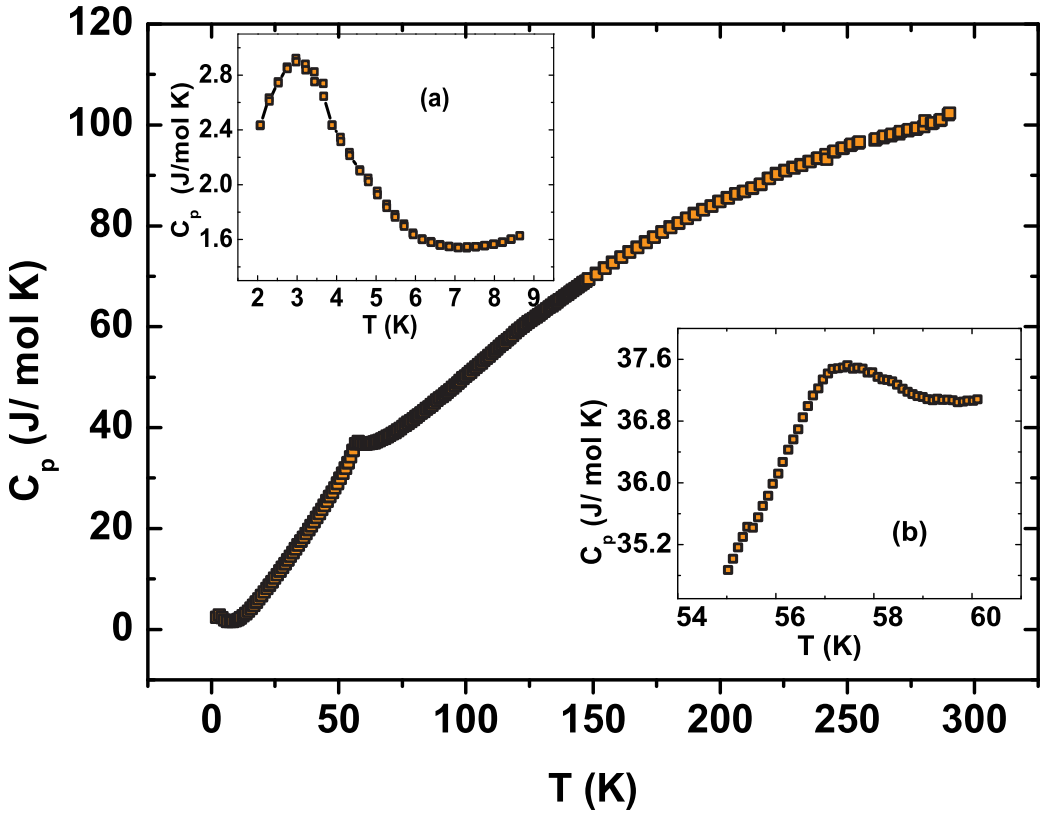

Figure 8: Specific heat at zero applied field for h-$DyMnO_3$. The insets magnify (a) the low temperature peak and (b) the peak at the Mn antiferromagnetic transition.

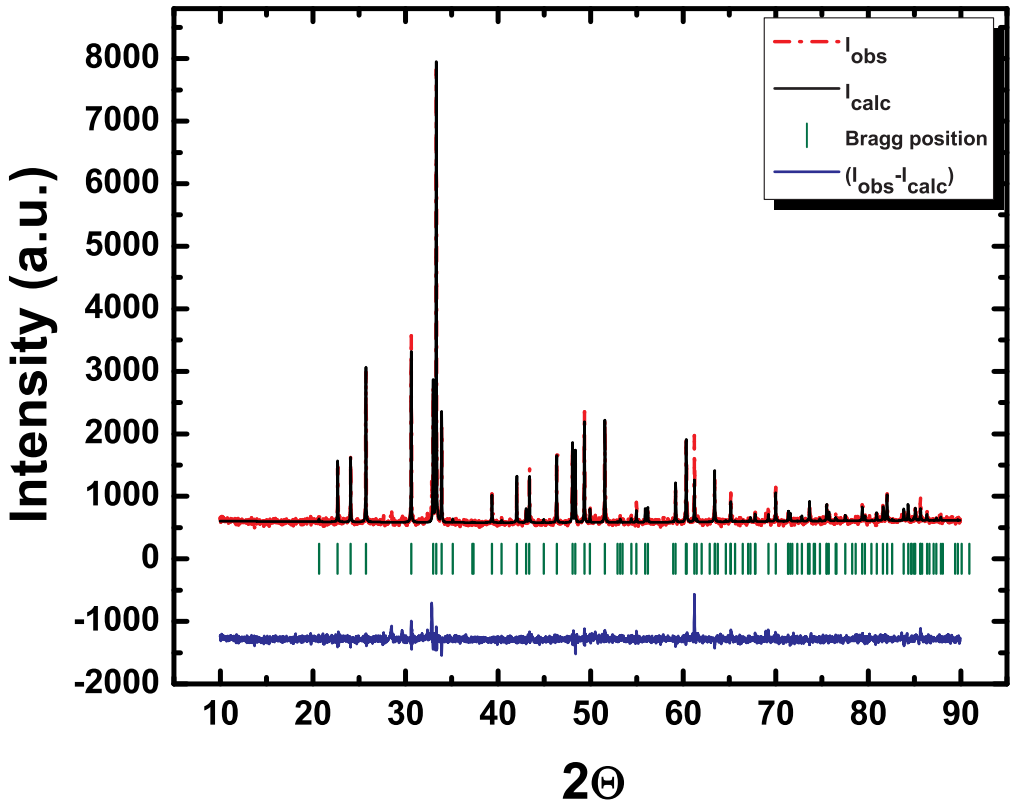

Figure 9: The powder X-ray diffraction pattern (I_{obs}) and the Rietveld refinement (I_{calc}) of o-$DyMnO_3$.

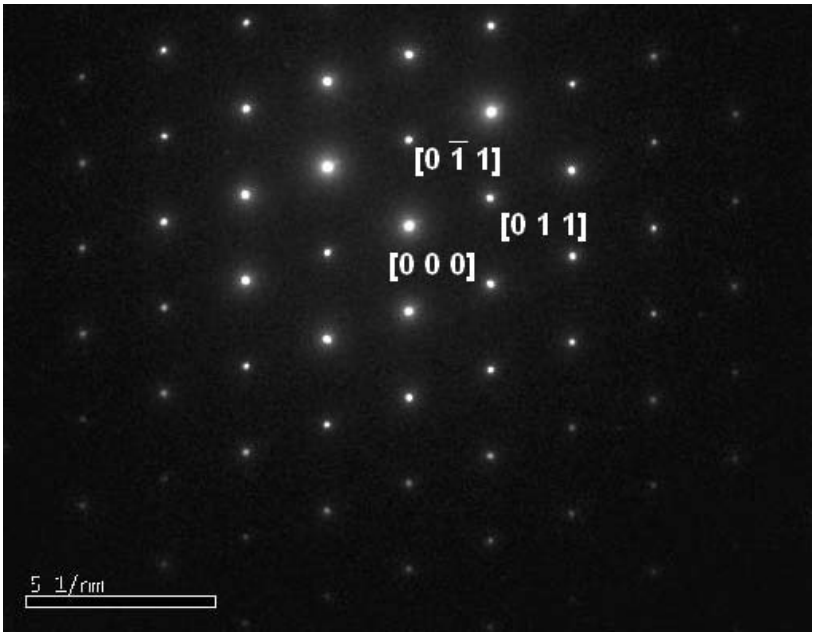

Figure 10: SAED pattern of o-$DyMnO_3$. The scale bar shows 5 nm^{-1}.

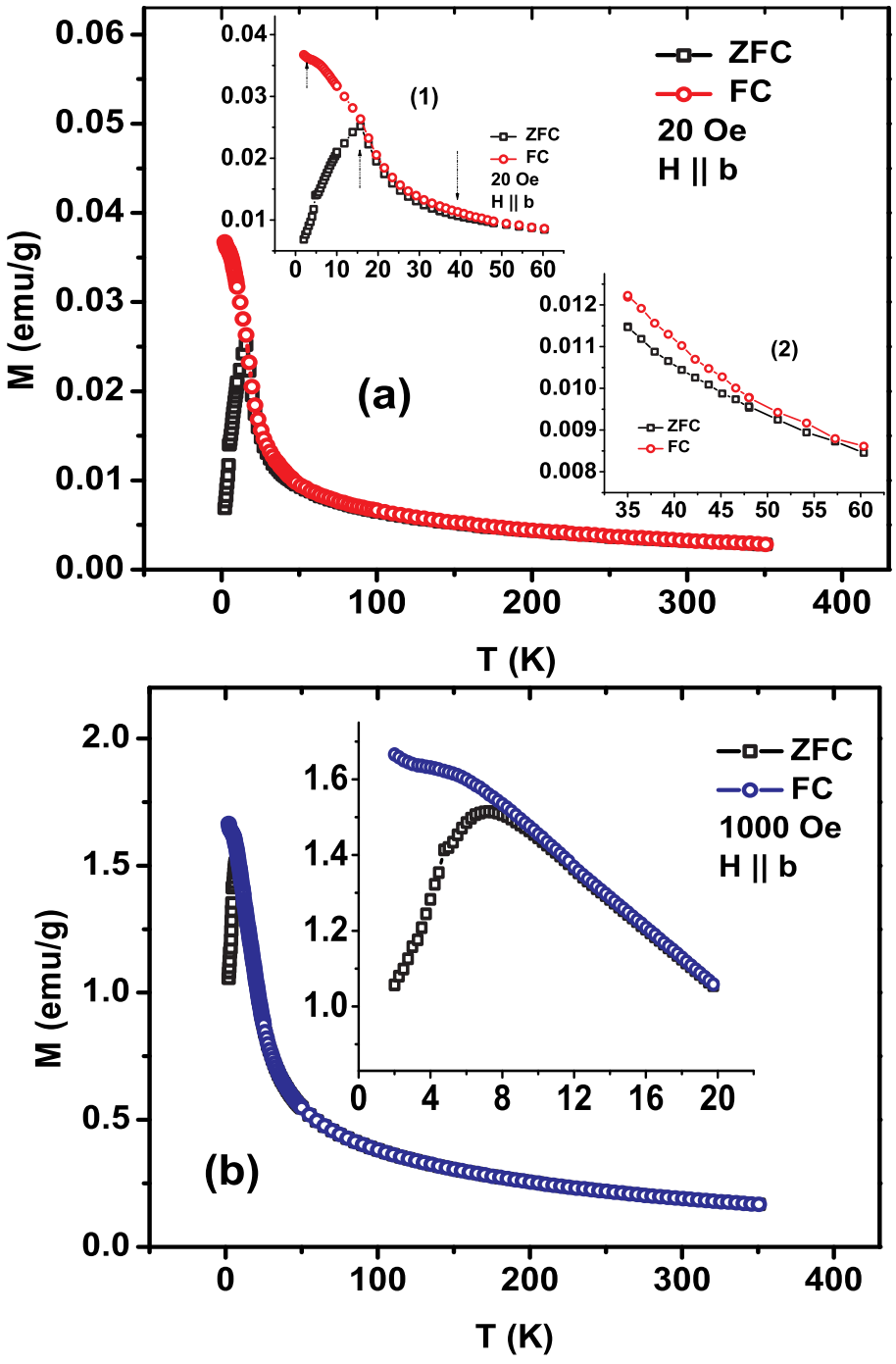

Figure 11: Magnetisation in dependence on temperature of o-$DyMnO_3$ *parallel* to b axis with (a) H = 20 Oe and (b) H = 1000 Oe. The three transitions described in the text are indicated by arrows in the inset 1 of (a). Inset 2 of (a) magnifies the ZFC-FC bifurcation around 45 K. The peak in the ZFC magnetization shifted to lower temperatures in higher applied field can be clearly seen in the inset of (b).

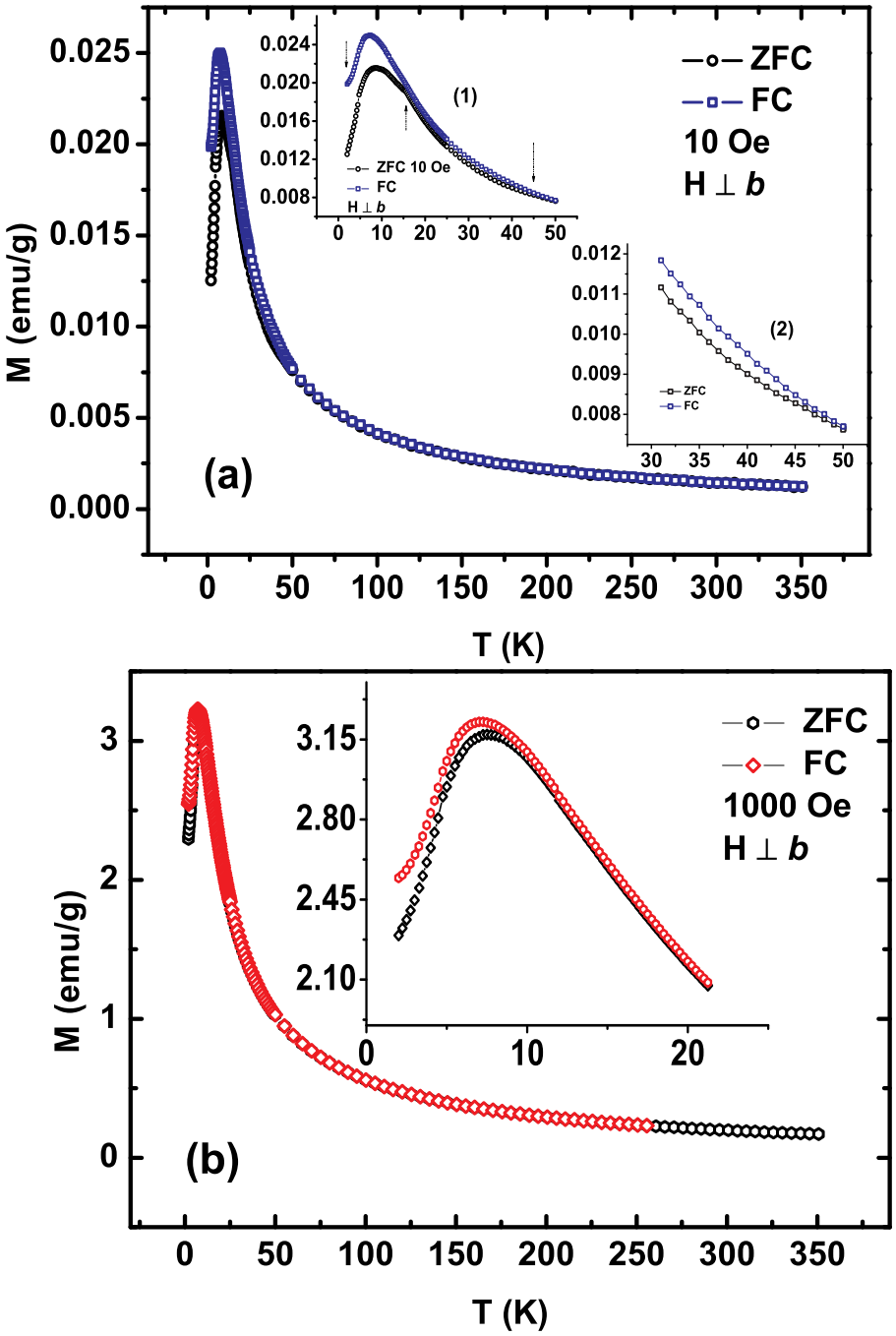

Figure 12: Magnetisation of o-$DyMnO_3$ *perpendicular* to b axis with (a) H = 10 Oe and (b) H = 1000 Oe. The three transitions described in the text are indicated by arrows in the inset 1 of (a). Inset 2 of (a) magnifies the ZFC-FC bifurcation around 45 K. Inset of (b) magnifies the magnetization with H = 1000 Oe at temperatures below 20 K.

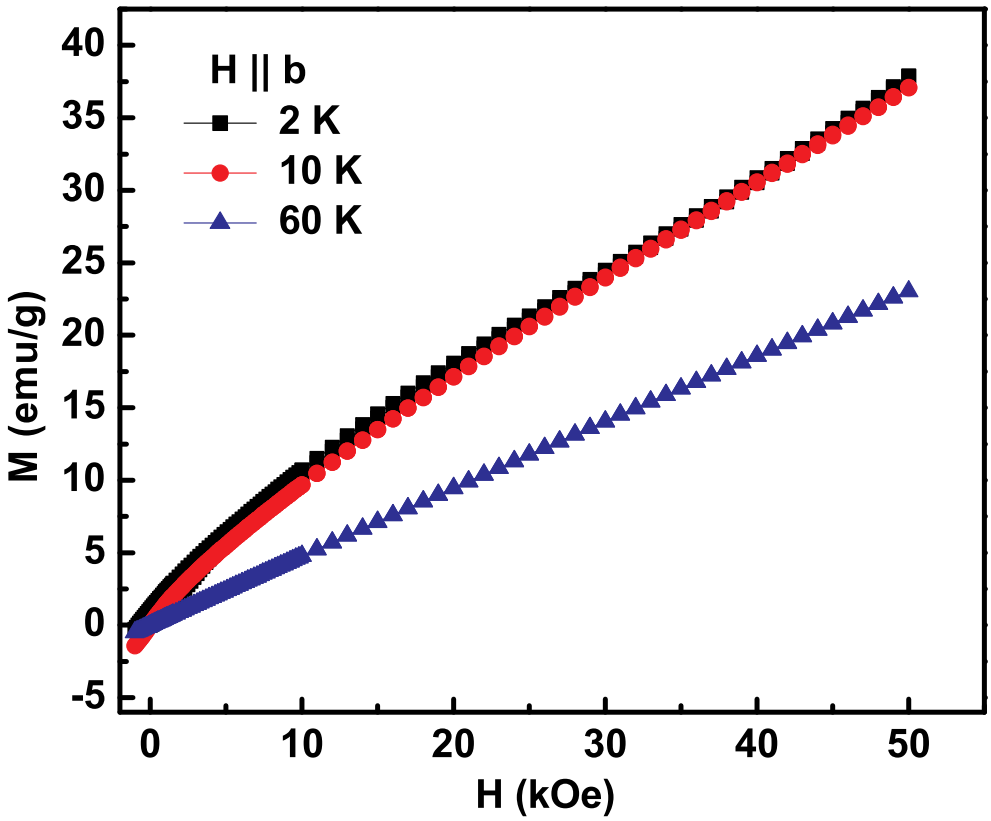

Figure 13: Magnetisation of o-$DyMnO_3$ at 2, 10 and 60 K with magnetic field parallel to b-axis

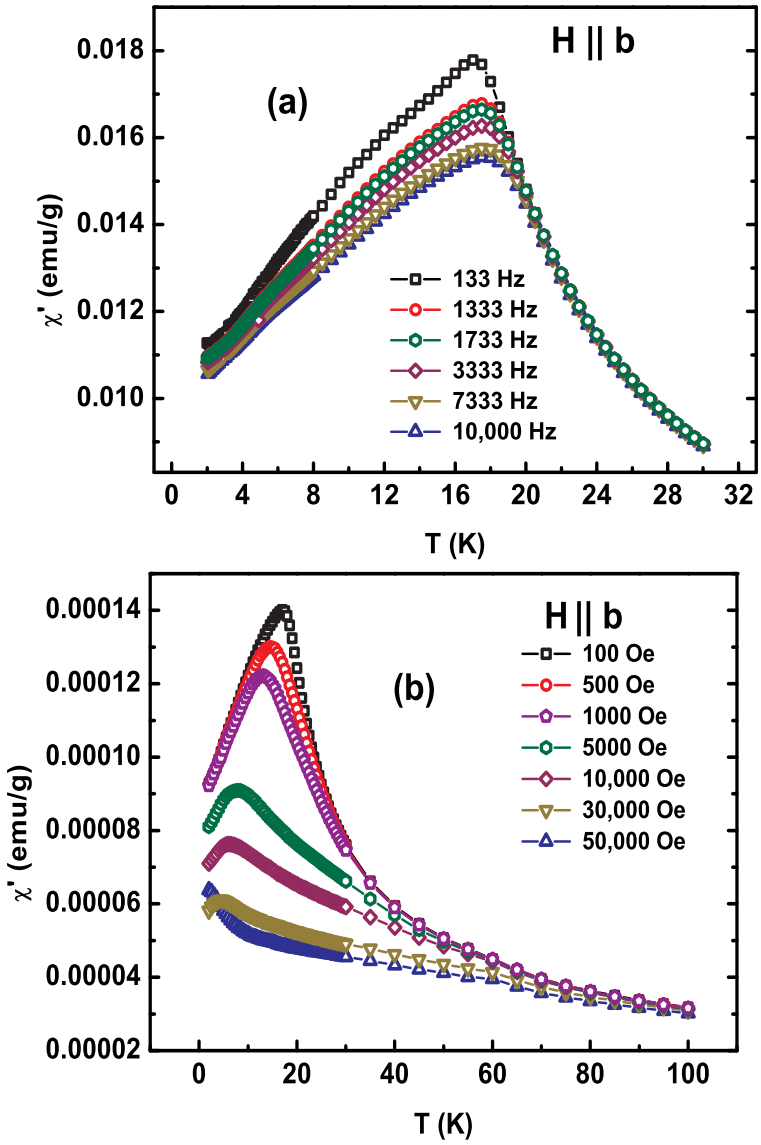

Figure 14: (a) The temperature dependence of ac susceptibility χ' at different frequencies measured with an ac field amplitude of 10 Oe. (b) The effect of an imposed magnetic field on the susceptibility of o-$DyMnO_3$ measured in a frequency of 1333 Hz and an ac field amplitude of 10 Oe.

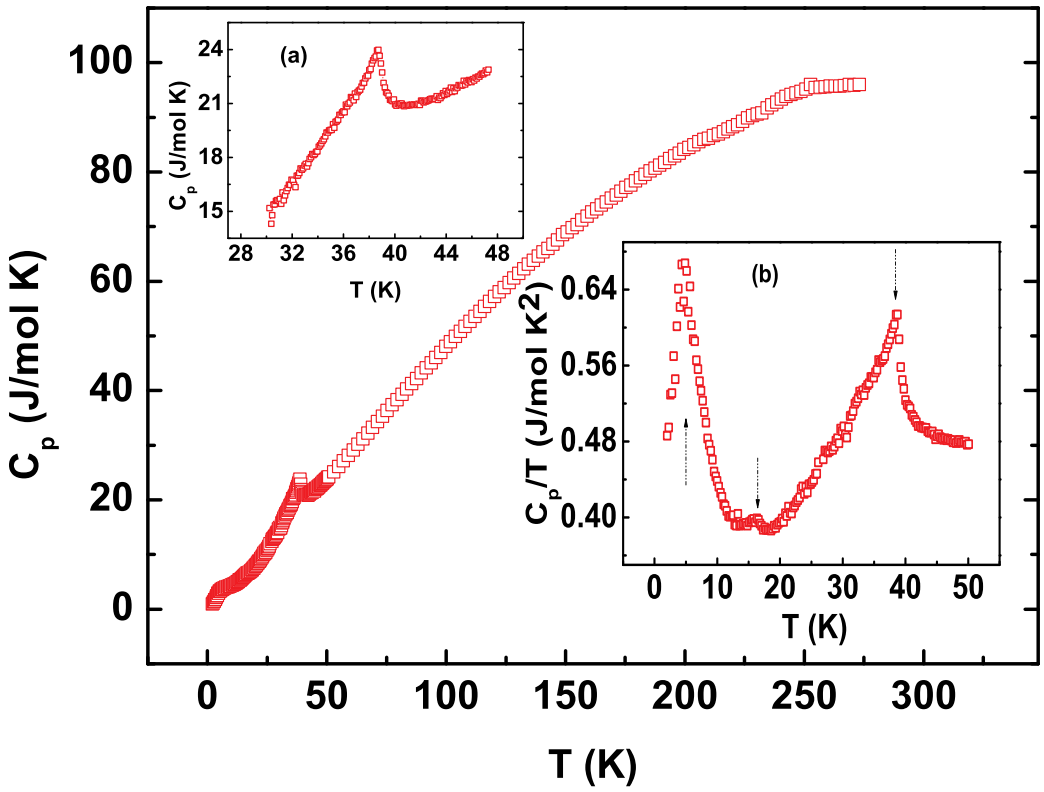

Figure 15: Specific heat at zero applied field for o-$DyMnO_3$. The insets show (a) the high temperature peak at the magnetic ordering transition for the Mn-sublattice at T_N^{Mn}. (b) the C_p/T plot indicating the $l$ock–in transition at $T_{lock-in} \approx 16$ K.